DOI: 10.1478/AAPP.97S1A18

AAPP | Atti della Accademia Peloritana dei Pericolanti
Classe di Scienze Fisiche, Matematiche e Naturali
ISSN 1825-1242

Vol. 97, No. S1, A18 (2019)

HYDRODYNAMIC MODELING OF ELECTRON TRANSPORT IN GATED SILICON NANOWIRES TRANSISTORS

ORAZIO MUSCATO [a], TINA CASTIGLIONE [a] AND ARMANDO COCO [ab*]

ABSTRACT. We present a theoretical study of the low-field electron mobility in rectangular gated silicon nanowire transistors at 300 K based on a hydrodynamic model and the self-consistent solution of the Schrödinger and Poisson equations. The hydrodynamic model has been formulated by taking the moments of the multisubband Boltzmann equation, and closed on the basis of the Maximum Entropy Principle. It includes scattering of electrons with acoustic and non-polar optical phonons and surface roughness scattering.

1. Introduction

As transistor sizes shrink down to the nanoscale, alternative structures and devices have been investigated during these years. Existing Metal-Oxide Semiconductor Field Effect Transistors (MOSFET) are expected to evolve from planar to 3-D nonplanar devices at nanometer sizes. A possible device approach that has attracted much attention recently because of its possibility of enhanced electrostatic control, is the use of nanowire transistors. Nanowire transistors of diameters even down to 3 nm have already been demonstrated by various experimental groups (Guerfi and Larrieu 2016; Singh *et al.* 2006). For engineering applications it is important to understand accurately electronic transport at the temperature at which circuits usually operate (300 K). Transport in such semiconductor nanowires is quasi-1D, because electrons are confined in two transverse directions and they are free to move only along the axis of the wire. It has been proved that the main quantum transport phenomena in nanowires at room temperature, such as the source-to-drain tunneling, and the conductance fluctuation induced by the quantum interference, become significant only when the length of the wire is smaller than 10 nm (Wang and Lundstrom 2002). Therefore, for longer lengths, semiclassical formulations based on the 1-D multisubband Boltzmann Transport Equation (MBTE) can give reliable terminal characteristics when it is solved self-consistently with the 3-D Poisson and 2-D Schrödinger equations in order to get the self-consistent potential, subband energies and wavefunctions. During these years, numerical solutions of the MBTE have been obtained using Direct Simulation Monte Carlo (Lenzi *et al.* 2008; Ramayya and Knezevic 2010; Ramayya *et al.* 2008), or deterministic solvers (Jin, Fischetti, and Tang 2007; Lenzi *et al.* 2008; Ossig and Schürrer 2008), at expense of

huge computational efforts and statistical noise (Muscato, Di Stefano, and Wagner 2013; Muscato and Wagner 2016; Muscato, Wagner, and Di Stefano 2010, 2011).

In alternative, hydrodynamical models can be obtained from the moment equations of the MBTE suitably truncated at a certain order. The truncation procedure requires solving the following two important problems: (i) the closure problem, and (ii) the modeling of the production terms. These problems can be tackled by means of the Maximum Entropy Principle (hereafter MEP) of Extended Thermodynamics (Lebon, Jou, and Casas-Vázquez 2008; Mascali and Romano 2010, 2012), in which the distribution function used to calculate the higher-order moments and the production terms is assumed to be that which maximizes the entropy under the constraints of the given set of moments. We want to underline that the distribution function obtained with the MEP is an approximation of the real one but, from the other side, this distribution is useful to determine analytically without any fitting procedure the higher-order moments and the production terms.

Taking advantage of this methodology, recently a new hydrodynamic model for Silicon Nanowires (SiNW) has been obtained (Castiglione and Muscato 2017; Muscato and Castiglione 2016; Muscato and Di Stefano 2012, 2014). In this paper we shall adopt this model for studying charge transport in Silicon Nanowire Transistors (SiNWT), where the nanowire transistor is a nanowire with an added gate.

2. Quantum confinement

In bulk Silicon (Si) the lowest conduction band is formed by six equivalent valleys near the X-point of the Brilloiun zone. In SiNW the band structure is altered with respect to the bulk case depending on the cross-section wire dimension, the atomic configuration, and the crystal orientation Neophytou *et al.* 2008. Since we want to skip all the difficulties introduced by the real band structure, and concentrate into the numerical issues, in this paper we shall employ a single valley, with an effective mass $m^* = 0.32\ m_e$, m_e being the free electron mass.

In the following, we shall consider a SiNW in which electrons are spatially confined in the x-y plane and are free to move in the orthogonal z direction, having dimension L_z. Hence, it is natural to assume the following ansatz for the electron wave function

$$\phi(x,y,z) = \chi_\nu(x,y)\frac{e^{ik_z z}}{\sqrt{L_z}} \tag{1}$$

where $\chi_\nu(x,y)$ is the wave function of the ν-th subband and the term $e^{ik_z z}/\sqrt{L_z}$ describes an independent plane wave in z-direction confined to the normalization length, with wave number k_z. The conduction electrons moving in the wire will react to the confining potential $U(x,y)$, such as by a discontinuity in the band gap at an interface between two materials, and to the presence of all other free electrons in the system. The simplest approximation which takes into account the presence of many electrons, called *Hartree approximation*, is to assume that the electrons as whole produce an average electrostatic potential energy V, and that a given electron feels the resulting total potential energy V_{tot}, i.e.

$$V_{tot}(x,y,z) = U(x,y) - eV(x,y,z) \tag{2}$$

where e is the absolute value of the electric charge.

The spatial confinement in the (x,y) plane is governed by the Schrödinger-Poisson system (SP). The electron wavefunction and energy level of each subband are obtained by solving the Schrödinger equation in the Effective Mass Approximation with $V_{tot}(x,y,z)$, in each z-th cross section of the device

$$\begin{cases} H[V]\,\chi_{\nu z}[V] = \varepsilon_{\nu x}[V]\,\chi_{\nu z}[V] \\ \\ H[V] = -\dfrac{\hbar^2}{2m^*}\left(\dfrac{\partial^2}{\partial x^2}+\dfrac{\partial^2}{\partial y^2}\right)+U-eV \end{cases} \tag{3}$$

which is coupled to the Poisson equation

$$\nabla\cdot[\varepsilon_0\varepsilon_r\nabla V(x,y,z)] = -e(N_D-N_A-n[V]) \tag{4}$$

where the electron density is

$$n[V](x,y,z,t) = \sum_\nu \rho_\nu(z,t)|\chi_{\nu z}[V](x,y,t)|^2 \tag{5}$$

ε_0 is the absolute dielectric constant, ε_r is the relative dielectric constant, and N_D, N_A are the assigned doping profiles (due to donors and acceptors). The total electron energy is the sum of the quantized energy in the ν-th subband and the free-motion energy which, in the quasi-parabolic band approximation, writes

$$E_\nu = \varepsilon_{\nu z}+\mathscr{E}_z(k_z), \quad \mathscr{E}_z(k_z)\,[1+\alpha\mathscr{E}_z(k_z)] = \frac{\hbar^2k_z^2}{2m^*}$$

where α = 0.5 eV^{-1}. The parabolic band approximation is obtained by setting $\alpha = 0$. The term ρ_ν is the linear density in the ν-subband

$$\rho_\nu(z,t) = \frac{2}{2\pi}\int f_\nu(z,k_z,t)dk_z \tag{6}$$

which must be evaluated by the transport model in the free movement direction.

Moreover we shall assume that the cross-section Ω of the wire is surrounded by an oxide which gives rise to a deep potential barrier,

$$U(x,y) = \begin{cases} 0 \quad \text{if (x,y)} \in \Omega \\ 4.05 \quad \text{eV} \quad \text{otherwise.} \end{cases} \tag{7}$$

where 4.05 is the height of the energy barrier at the Si-oxide interface.

3. Kinetic transport equations

We have implicitly assumed that the description of low-dimensional systems in terms of the solutions of the effective mass equation is still a good solution to the problem in the presence of disorder. The use of the effective mass approximation is probably valid for semiconductor nanowires down to 5 nm in diameter, below which atomistic electronic structure models need to be employed (Zheng *et al.* 2005). In low-dimensional systems, we consider the perfect system to be defined by the static lattice, with perfectly smooth boundaries defining the system, free of impurities or other random inhomogeneities. Moreover we assume that the broadening of the energy levels due to disorder (i.e. the real part of the self energy) is small, so that crystal momentum conservation is approximately

preserved. In this weak coupling limit, we can then construct a kinetic equation in which the particle density function (or distribution function) evolves in time under the streaming motion of external forces and spatial gradients, and the randomizing influence of nearly point-like (in space-time) scattering events.

If the characteristic length of the device is order of tens of nanometers, the transport of electrons in the z-direction can be considered semiclassical within a good approximation. In a quantum wire, the quantum mechanical confinement splits up the band into subbands. Electrons in each subband are considered as different populations whose dynamics is described by a semiclassical distribution function, obeying to different Boltzmann equations. Therefore the description of electron in the transversal direction is included by adding the Schrödinger-Poisson equations. The distribution function for the electrons in a quantum wire, with linear expansion in z-direction, depends on the z-direction in real space, the wave vector in z-direction k_z and the time t, i.e.

$$f_\nu = f_\nu(z, k_z, t)$$

for each subband (ν). The MBTE reads (Ferry, Goodnick, and Bird 2009)

$$\frac{\partial f_\nu}{\partial t} + v_z(k_z)\frac{\partial f_\nu}{\partial z} - \frac{1}{\hbar}E_{eff}\frac{\partial f_\nu}{\partial k_z} = \sum_{\nu'}\sum_{\eta}\mathscr{C}_\eta[f_\nu, f_{\nu'}] \tag{8}$$

where $\hbar$ is the Planck constant divided by 2π, and v_z the group velocity

$$v_z = \frac{1}{\hbar}\frac{\partial E_{\nu z}}{\partial k_z} = \frac{\hbar k_z}{m^*[1+2\alpha\mathscr{E}_z(k_z)]}, \quad E_{eff} = -\frac{1}{e}\frac{\partial E_{\nu z}}{\partial z} \tag{9}$$

In the low density approximation (not-degenerate case), the collisional operator writes

$$\mathscr{C}_\eta[f_\nu, f_{\nu'}] = \frac{L_x}{2\pi}\int dk'_z\left\{w_\eta(\mathsf{k}',\mathsf{k})f_{\nu'}(k'_z) - w_\eta(\mathsf{k},\mathsf{k}')f_\nu(k_z)\right\} \tag{10}$$

where $w_\eta(\mathsf{k},\mathsf{k}') = w_\eta(\nu, k_z, \nu', k'_z)$ is the η-th scattering rate. When $\nu = \nu'$ we have an intra-subband scattering, otherwise we have an inter-subband scattering. In our model we have included the following scattering rates:

- Bulk acoustic phonon. In the elastic equipartition approximation, the transition rate is (Ferry, Goodnick, and Bird 2009)

$$w_{ac}(\mathsf{k},\mathsf{k}') = s_{ac}G^{\nu\nu'}\delta(E_{\nu'} - E_\nu) \quad , \quad s_{ac} = \frac{2\pi D_A^2 k_B T_L}{\rho\hbar v_s^2 L_z} \tag{11}$$

where D_A is the acoustic deformation potential (9 eV), T_L the lattice temperature, ρ the mass density (2.33 g/cm^3), v_s the sound speed (6960 m/s), and $G^{\nu\nu'}$ the confinement factor

$$G^{\nu\nu'} = \int |\chi_{\nu'}(x,y)|^2|\chi_\nu(x,y)|^2 dxdy \quad . \tag{12}$$

- Optical phonons. In this case

$$w_{op}(\mathsf{k},\mathsf{k}') = s_{op}\left[g_0 + \frac{1}{2} \mp \frac{1}{2}\right]G^{\nu\nu'}\delta(E_{\nu'} - E_\nu \mp \hbar\omega_0) \quad , \quad s_{op} = \frac{\pi D_0^2}{\rho\omega_0 L_z} \tag{13}$$

where D_0 is the optical deformation potential (11.4 10^8 eV/cm), $\hbar\omega_0$ the effective optical phonon energy (63 meV), and g_0 the Bose-Einstein phonon occupation number.

- Surface roughness scattering (SRS). In silicon nanowires it is the key scattering mechanism as it yields a very strong dependence of the low-field electron mobility on the silicon transversal dimension as well as on the effective field. If we consider the wire interface along the x-z plane (whose normal is the y direction), then $\Delta(x,z)$ is a random function which describes the deviation of the actual interface from the ideal flat interface. This fluctuation changes directly the confining potential U, and it induces a change in the other potentials. Therefore, the subband wave functions and energy bands depend explicitly from x. Following Ferry, Goodnick, and Bird (2009) and Ramayya *et al.* (2008) we shall consider a simpler model, in which the SRS accounts for deformations only for the potential V (not the wave functions), where the matrix element is

$$H_{sr} = eE_y(x,z)\Delta(x) \tag{14}$$

$E_y = -\partial V/\partial y$ being the electric field normal to the surface. In this case we have

$$\begin{aligned} w_{sr}(k_z,k_z',E_y) &= \frac{4\sqrt{2}e^2 m^*}{\hbar^3 L_z}\frac{\Theta(a)}{\sqrt{a}}[\mathscr{F}_{\nu\nu'}(E_y)]^2 \frac{\lambda\Delta^2}{(k_z-k_z')^2\lambda^2+2}\times \\ &\left[\delta\left(k_z'-\sqrt{a}\right)+\delta\left(k_z'+\sqrt{a}\right)\right] \end{aligned} \tag{15}$$

where $\Theta(x)$ is the Heaviside function, Δ (0.3 nm) the root mean square value of the roughness fluctuations, λ (1.5 nm) the autocovariance length which roughly may be interpreted as the mean distance between bumps along the surface, and

$$a = k_z^2 + \frac{2m^*}{\hbar}(\varepsilon_\nu - \varepsilon_{\nu'}), \quad \mathscr{F}_{\nu\nu'}(E_y) = \int \chi_\nu^\star(x,z)E_y(x,z)\chi_{\nu'}(x,z)\,dxdz. \tag{16}$$

4. The moment system and its closure by the MEP

By multiplying eq. (8) by the weight functions $(1, v_z, \mathscr{E}_z, \mathscr{E}_z v_z)$ and integrating over $2/(2\pi)dk_z$, one can obtain the following balance equations for the macroscopic quantities associated to the flow (Castiglione and Muscato 2017)

$$\frac{\partial\rho^\nu}{\partial t} + \frac{(\rho^\nu V^\nu)}{\partial z} = \rho^\nu \sum_{\nu'} C_\rho^{\nu\nu'}, \tag{17}$$

$$\frac{\partial(\rho^\nu V^\nu)}{\partial t} + \frac{\partial(\rho^\nu U^\nu)}{\partial z} + \frac{e}{\hbar}\rho^\nu E_{eff} R^\nu = \rho^\nu \sum_{\nu'} C_V^{\nu\nu'}, \tag{18}$$

$$\frac{\partial(\rho^\nu W^\nu)}{\partial t} + \frac{\partial(\rho^\nu S^\nu)}{\partial z} + \rho^\nu e E_{eff} V^\nu = \rho^\nu \sum_{\nu'} C_W^{\nu\nu'}, \tag{19}$$

$$\frac{\partial(\rho^\nu S^\nu)}{\partial t} + \frac{\partial(\rho^\nu F^\nu)}{\partial z} + \frac{e}{\hbar}\rho^\nu E_{eff} G^\nu = \rho^\nu \sum_{\nu'} C_S^{\nu\nu'}, \tag{20}$$

where ρ^ν is the subband density, V^ν the subband velocity, W^ν the subband energy, S^ν the subband energy-flux, $U^\nu, R^\nu, G^\nu, F^\nu$ are the higher-order fluxes, and $C_\rho^{\nu\nu'}$, $C_V^{\nu\nu'}$, $C_W^{\nu\nu'}$, $C_S^{\nu\nu'}$ are the production terms (i.e. the moments over the collisional operator). The moment

equations (17-20) do not constitute a set of closed relations. If we assume as fundamental variables $(\rho^\nu, V^\nu, W^\nu, S^\nu)$, which have a direct physical interpretation, the closure problem consists in expressing the high-order fluxes and the production terms as function of the fundamental variables. The Maximum Entropy Principle (MEP) gives a systematic way for obtaining constitutive relations on the basis of information theory (Lebon, Jou, and Casas-Vázquez 2008; Mascali and Romano 2010, 2012) and has been widely used in the simulation of 2D nanoscale structures (Camiola, Mascali, and Romano 2012, 2013), and for simulating the 3D electron transport in sub-micrometric devices, in the case in which the lattice is considered as a thermal bath with constant temperature (Di Stefano and Muscato 2012; Muscato and Di Stefano 2011d) or when the phonons are off-equilibrium (Mascali 2015, 2016, 2017; Muscato and Di Stefano 2011a,b,c, 2013, 2015). According to the MEP, if a given number of moments are known, the distribution function $\hat{f}$, which can be used to evaluate the unknown moments, corresponds to the extremum of the total entropy density under the constraint that they yield the known moments. In this way one obtains the following distribution function which is function of the prescripted moments, *i.e.*

$$\hat{f}_\nu = \exp\left(-\frac{\lambda^\nu}{k_B} - \lambda_W^\nu \mathscr{E}_z\right)\left\{1 - \tau\left(\hat{\lambda}_V^\nu v_z + \hat{\lambda}_S^\nu v_z \mathscr{E}_z\right)\right\}, \tag{21}$$

where the quantities $(\lambda^\nu, \lambda_W^\nu, \hat{\lambda}_V^\nu, \hat{\lambda}_S^\nu)$ are known functions of the fundamental variables $\{\rho^\nu, V^\nu, W^\nu, S^\nu\}$. By using the MEP distribution function (21) one can evaluate the unknown functions appearing in the balance equations by integration such as the higher-order flux terms and the production terms (Castiglione and Muscato 2017; Muscato and Castiglione 2017). In this way a *physics-based* hydrodynamic model has been obtained, which is free of tunable parameters.

5. Silicon Nano Wire Transistor

The SiNWT considered in this study has a parallelepiped geometry with a metal gate wrapped around it, in such a way we have a three contact device with source, drain, gate (see Figure 1) called Gate-All-Around SiNWT. Such devices have been designed during these years in order to maintain a good electrostatic control in the channel (Guerfi and Larrieu 2016). In the following we shall consider a very simple SiNWT having the channel homogeneously doped to $N_D = 3\ 10^{15}\,\mathrm{cm}^{-3}$ and very long (L_z = 120 nm) with respect to the transversal dimensions ($L_x = L_y = 10$ nm), where the oxide thickness is tox = 1 nm.

Our aim is to determine the low-field mobility, which has a surprisingly strong influence on the performance of short-channel devices. For this reason, it is still used as a figure of merit for benchmarking different technology options and device architectures. We fix an uniform electric field F along the channel of 1 kV/cm, and then we compute the low-field mobility

$$\mu_{low} = \frac{1}{F}\frac{\sum_\nu \rho_\nu V_\nu}{\sum_\nu \rho_\nu} \tag{22}$$

as a function of the gate voltage V_G. The subband density ρ_ν and velocity V_ν are determined with the following steps (Ramayya and Knezevic 2010):

(1) **equilibrium solution**
First of all we determine the thermal equilibrium condition, which is obtained when

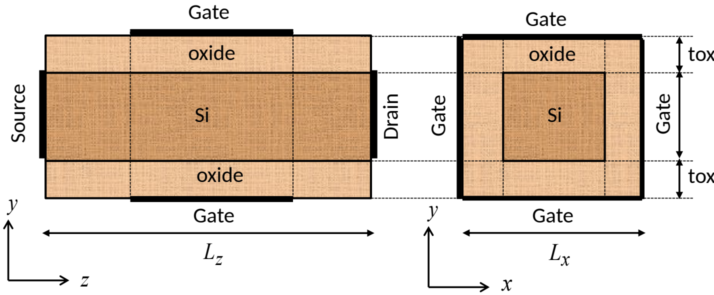

FIGURE 1. Cross sections of a GateAllAroundSiNWtransistor.

no voltage is applied to the contacts, i.e. $V_S = V_D = V_G = 0$, and no current flows. In this case the electron distribution function is the maxwellian,

$$f_\nu^{(eq)}(k_z) = N_0 \exp\left(-\frac{\frac{\hbar^2 k_z^2}{2m^*} + \varepsilon_\nu - E_F}{k_B T}\right) \tag{23}$$

where E_F is the Fermi level and T the electron temperature which we shall assume to be the same in each subband and equal to the lattice temperature. The condition of zero net current requires that the Fermi level must be constant throughout the sample, and it can be determined by imposing that the total electron number equals to the total donor number in the wire. Then, the linear density (6) at equilibrium writes

$$\rho_\nu^{(eq)}(z) = \frac{N_D L_x L_y}{\mathscr{Z}^{(eq)}} \exp\left[\frac{-\varepsilon_{\nu z}^{(eq)}}{k_B T}\right], \quad \mathscr{Z}^{(eq)} = \sum_\nu \exp\left[\frac{-\varepsilon_{\nu z}^{(eq)}}{k_B T}\right] \tag{24}$$

where the subband energies $\varepsilon_{\nu z}^{(eq)}$ are obtained by solving the SP system (3)-(5) using eq. (24). The SP solver has been described in the Appendix A.

(2) **quasi-equilibrium solution**
Now we consider the quasi-equilibrium regime, where a very small axial electric field frozen along the channel (1kV/cm) is applied, and we turn on the gate. In such a case the system is still in local thermal equilibrium, the distribution function is

the maxwellian, but some charge flows in the wire. The linear density writes

$$\rho_\nu(z) = \frac{N_D L_x L_y}{\mathscr{Z}^{(eq)}} \exp\left[-\frac{\varepsilon_{\nu z}}{k_B T}\right] \tag{25}$$

where the only difference between eqs. (24), (25) is in the energy subbands $\varepsilon_{\nu z}$, which now are obtained solving the SP system (3)-(5) with $V_S = 0.012$ V, $V_D = 0$ V, and for some values of V_G.

(3) **charge transport determination**
The charge transport is governed by the hydrodynamic model (17)-(20). Since the wire is uniformly doped, with a frozen electric field along its z-axis, we can skip the spatial dependence in this model, which reduces to a system of Ordinary Differential Equations.
The energies $\varepsilon_{\nu z}$ and wave functions $\chi_{\nu z}$ for each subband are imported from the previous steps (and kept fixed), as well as the linear density (25) which is used as initial condition. The other initial conditions are

$$V_\nu(0) = 0, \quad W_\nu(0) = \frac{1}{2} k_B T, \quad S_\nu(0) = 0 \quad . \tag{26}$$

The hydrodynamic system has been solved using a standard Runge-Kutta algorithm. The simulation stops when the stationary regime has been reached obtaining the subband densities and velocities, and finally the low-field mobility (22) has been evaluated.

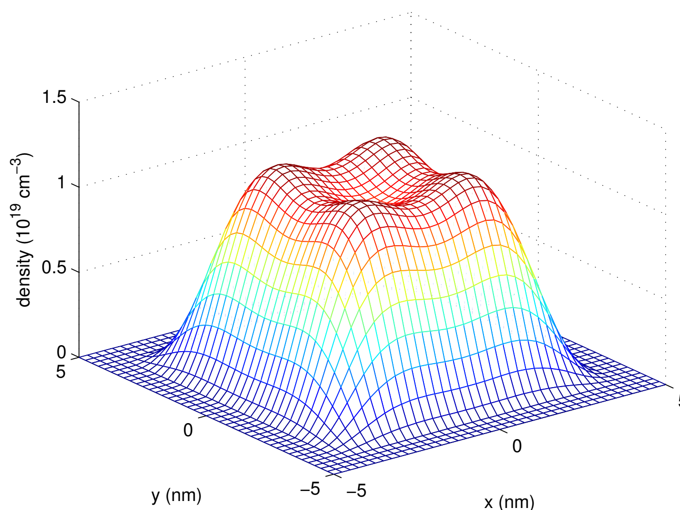

FIGURE 2. Electron density (5) in the cross-section at z = 72 nm, under a 0.3 V gate bias.

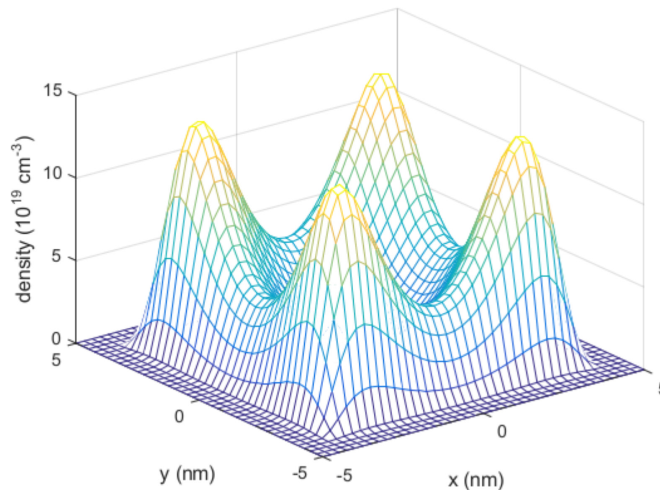

FIGURE 3. Electron density (5) in the cross-section at z = 72 nm, under a 1 V gate bias.

Figures 2-3 show the electron density (5) obtained with gate voltage V_G = 0.3 and 1 respectively, in a transversal cross-section of the SiNWT. For V_G = 0.3 V, the geometrical well confinement is dominant and the volume charge is peaked around the center of the wire, as shown in Figure 2. For V_G = 1 V, a surface inversion layer is formed, similar to a usual MOSFET channel with the electron density peaked close to the oxide interface (see Figure 3). The bandbending at the interface forms the quantum well for electrons, which has a characteristic signatures in the mobility.

In Figure 4 we plot the low-field mobility versus the gate bias V_G, obtained in the parabolic band approximation and by including/excluding the Surface Roughness Scattering mechanism (15). From this Figure one can see how is fundamental such scattering mechanism especially for large gate voltage, when the surface inversion layer is formed. Similar results are shown in Figure 5 obtained in the quasi-parabolic band approximation. The effect of the quasi-parabolic band approximation is to lower the low-field mobility with respect to the parabolic case. These results are in qualitative agreement with simulations available in literature (Lenzi *et al.* 2008; Ramayya and Knezevic 2010), proving that our model works in an appropriate manner. We remember that our model has been implemented using a single conduction valley, and the results can change with a more realistic band structure. The problem of identifying the appropriate band structure in SiNW as a function of geometry and crystal orientation has been addressed by means of atomistic simulations, obtaining a variety of theoretical studies with non unique solutions (Gnani *et al.* 2007; Nehari *et al.* 2006; Neophytou and Kosina 2011).

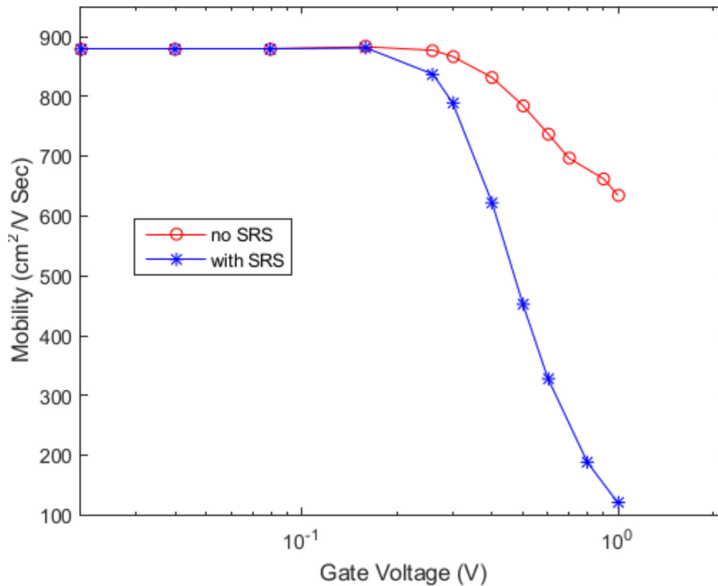

FIGURE 4. Low-field mobility (22) versus the gate voltage (V_G), obtained in the parabolic band approximation.

6. Conclusions

In this paper we have introduced a hydrodynamic model coupled to the Schrödinger-Poisson equations, to study the charge transport in SiNWT. The hydrodynamic model has been formulated by taking the moments of the multisubband Boltzmann equation, and by closing the obtained hierarchy of balance equations with the use of the Maximum Entropy Principle. Relevant scattering mechanisms, such as scattering of electrons with acoustic and non-polar optical phonons and surface roughness, have been included. A self-consistent Schrödinger-Poisson-hydrodynamic solver has been developed to study the effect of 2D spatial confinement on the low-field mobility of electrons in a Gate-All-Around SiNWT. The obtained results show a good qualitative agreement with data available from the literature. The inclusion of a more realistic band structure in our model will be published in the next future.

Acknowledgments

We acknowledge the support of the Università degli Studi di Catania, FIR 2014 “Charge Transport in Graphene and Low dimensional Structures: modeling and simulation” and the National Group of Mathematical Physics (GNFM-INdAM), “Progetto giovani 2015”.

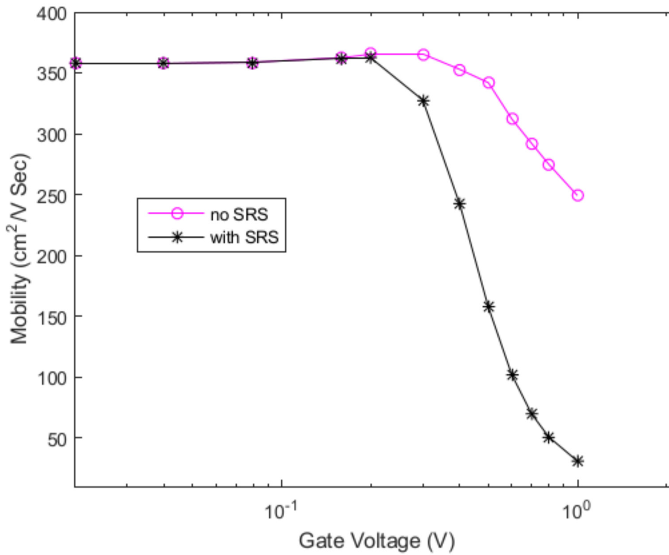

FIGURE 5. Low-field mobility (22) versus the gate voltage (V_G), obtained in the quasi parabolic band approximation.

Appendix A: the SP block solver

The SP system (3)-(5) forms a coupled nonlinear PDEs, which it is usually solved by an iteration between Poisson and Schrödinger equations. Since in a simple iteration by itself does not converge, it is necessary to introduce an adaptive iteration scheme. We have used a predictor-corrector type approach (Trellakis *et al.* 1997), where a modified Poisson equation has been introduced. The scheme will start using the equilibrium solution (24), i.e.

$$n^{(0)} = n^{(eq)}, \quad V^{(0)} = V^{(eq)} \quad .$$

(1) **For l=0: Niter.**
Solve the 3D Poisson equation (see Appendix B for the details) with a predicted density $\tilde{n}$

$$\begin{cases} \nabla \cdot \left[\varepsilon_0 \varepsilon_r \nabla V^{(l+1)} \right] = -e \left(N_D - N_A - \tilde{n} \left[V^{(l+1)}, V^{(l)} \right] \right) \\ \\ \tilde{n} \left[V^{(l+1)}, V^{(l)} \right] = n^{(l)} \exp \left[\dfrac{q(V^{(l+1)} - V^{(l)})}{k_B T} \right] \end{cases} \tag{27}$$

and obtain $V^{(l+1)}(x,y,z)$.

(2) For each z, solve Schrödinger equation

$$H[V^{(l+1)}]\chi_{\nu z}^{(l+1)} = \varepsilon_{\nu z}^{(l+1)} \chi_{\nu z}^{(l+1)} \tag{28}$$

and obtain $\varepsilon_{\nu z}^{(l+1)}, \chi_{\nu z}^{(l+1)}$.

(3) Evaluate the exact density

$$n^{(l+1)}(x,y,z) = \frac{N_D L_x L_y}{\mathscr{Z}^{(eq)}} \sum_{\nu} \exp\left[-\frac{\varepsilon_{\nu z}^{(l+1)}}{k_B T}\right] \left|\chi_{\nu z}^{(l+1)}\right|^2 \tag{29}$$

(4) IF

$$\frac{\left\| n^{(l+1)} - n^{(l)} \right\|_\infty}{\left\| n^{(l+1)} \right\|_\infty} < \text{tolerance} \tag{30}$$

EXIT (end l loop) ELSE **continue** (goto 1) .

If

$$\left\| \frac{q(V^{(l+1)} - V^{(l)})}{k_B T} \right\| \ll 1$$

we can expand the exp function, and the eq. (27) writes

$$\nabla \cdot \left[\varepsilon_0 \varepsilon_r \nabla V^{(l+1)}\right] = -e \left\{ N_D - N_A - n^{(l)} - \frac{q n^{(l)}}{k_B T} \left[V^{(l+1)} - V^{(l)}\right] \right\} \tag{31}$$

Appendix B: the Poisson equation solver

The equation for the potential $V^{(l+1)}$, in non dimensional form, is the following:

$$\nabla \cdot \left[\varepsilon_r(x,y,z) \nabla V^{(l+1)}\right] = \beta \left\{ n^{(l)}(x,y,z) \left[V^{(l+1)} - V^{(l)}\right] - N_D(x,y,z) \right\} \tag{32}$$

The potential is assigned on the gate and on the bottom and top surfaces (Dirichlet condition), while on the rest of the boundary we assume that the derivative of $V^{(l+1)}$ along the normal direction of the boundary is zero (Neumann condition). Therefore, the problem for the potential $V^{(l+1)}$ can be written as:

$$-\nabla \cdot \left[\varepsilon_r(x,y,z)\, \nabla V^{(l+1)}\right] + \delta\, V^{(l+1)} = f \quad \text{in} \quad \Omega \tag{33}$$

$$V^{(l+1)} = V \quad \text{on} \quad \Gamma_{bottom} \cup \Gamma_{top} \cup \Gamma_{gate} \tag{34}$$

$$\frac{\partial V^{(l+1)}}{\partial n} = 0 \quad \text{on} \quad \partial\Omega - (\Gamma_{bottom} \cup \Gamma_{top} \cup \Gamma_{gate}), \tag{35}$$

where $\delta = -\beta\, n^{(l)}(x,y,z)$, $f = \beta \left\{ n^{(l)}(x,y,z)\, V^{(l)} + N_D(x,y,z) \right\}$,
$\Omega = [a,b] \times [c,d] \times [e,f]$, $\Gamma_{bottom} = [a,b] \times [c,d] \times \{e\}$, $\Gamma_{top} = [a,b] \times [c,d] \times \{f\}$, $\Gamma_{gate} = \{(x,y,z) \in \partial\Omega \colon z_1 \le z \le z_2\}$.

The domain Ω is split into two subdomains Ω_i and Ω_e such that

$$\Omega_i = \{(x,y,z) \in \Omega \colon x^* \le x \le x^{**},\, y^* \le y \le y^{**}\}$$

where $a < x^* < x^{**} < b$, $c < y^* < y^{**} < d$) and $\Omega_e = \Omega - \Omega_i$. The coefficient function $\varepsilon_r(x,y,z)$ is discontinuous across $\Gamma = \partial\Omega_i - \partial\Omega$ and therefore the standard central finite-difference method (that is second order accurate on regions with smooth solutions) cannot be used to discretize Eq. (33) close to the interface $\partial\Omega_i$, since there is a jump in the derivative of $V^{(l+1)}$ across the interface that would degrade the order of accuracy. In order to employ

a finite-difference method that maintains the second order of accuracy (Coco and Russo 2012, 2013, 2018), a proper interface condition must be considered:

$$\lim_{\Omega_i \ni (x,y,z) \to (\bar{x},\bar{y},\bar{z})} \left(\varepsilon_r \frac{\partial V^{(l+1)}}{\partial n} \right) = \lim_{\Omega_e \ni (x,y,z) \to (\bar{x},\bar{y},\bar{z})} \left(\varepsilon_r \frac{\partial V^{(l+1)}}{\partial n} \right), \tag{36}$$

where $(\bar{x},\bar{y},\bar{z}) \in \Gamma$ and n is the normal direction to Γ.

The domain Ω is discretized by a uniform Cartesian grid:

$$(x_i, y_j, z_k),\ i = 0,\dots,n,\ j = 0,\dots,m,\ k = 0,\dots,p, \tag{37}$$

where $x_i = a + i\Delta x$, $y_j = c + j\Delta y$ and $z_k = e + k\Delta z$, with $\Delta x = (b-a)/n$, $\Delta y = (d-c)/m$ and $\Delta z = (f-e)/p$. The Cartesian grid is chosen in such a way that $x^* = x_{i^*}$, $x^{**} = x_{i^{**}}$, $y^* = y_{i^*}$, $y^{**} = y_{i^{**}}$ for some integers $2 \le i^* < i^{**} \le n-2$, $2 \le j^* < j^{**} \le m-2$.

The unknown function $V^{(l+1)}$ is therefore represented by a grid function defined over the cartesian grid (37), namely by a vector $\mathbf{v} \in \mathbb{R}^{(n+1)(m+1)(p+1)}$. The approximation of $V^{(l+1)}(x_i, y_j, z_k)$ is represented by the s-th component of the vector $\mathbf{v}$, with $s = 1 + i + (n+1)j + (n+1)(m+1)k$. We observe that the relation $s = 1 + i + (n+1)j + (n+1)(m+1)k$ represents a one-to-one map between the grid and the set of the first $(n+1)(m+1)(p+1)$ integers, i.e.:

$$\mathscr{M}:\ \{0,\dots,n\} \times \{0,\dots,m\} \times \{0,\dots,p\} \longrightarrow \{1,\dots,(n+1)(m+1)(p+1)\}, \tag{38}$$

$$\text{where} \quad \mathscr{M}(i,j,k) = 1 + i + (n+1)j + (n+1)(m+1)k. \tag{39}$$

In the following, we can use the notation v_{ijk} to refer to the vector component v_s, with $s = \mathscr{M}(i,j,k)$.

The vector $\mathbf{v}$ is found by solving a $(n+1)(m+1)(p+1) \times (n+1)(m+1)(p+1)$ linear system obtained as follows. Let s be a generic integer such that $1 \le s \le (n+1)(m+1)(p+1)$ and let (x_i, y_j, z_k) be the grid point corresponding to $\mathscr{M}^{-1}(s)$. If $(x_i, y_j, z_k) \in \Gamma_{bottom} \cup \Gamma_{top} \cup \Gamma_{gate}$ the s-th equation of the linear system is obtained from the Dirichlet boundary condition (34):

$$v_{ijk} = V(x_i, y_j, z_k).$$

If $(x_i, y_j, z_k) \in \partial\Omega - (\Gamma_{bottom} \cup \Gamma_{top} \cup \Gamma_{gate})$ the s-th equation of the linear system is obtained by discretizing the Neumann boundary condition (35) on (x_i, y_j, z_k) with second order accuracy as follows (assume that $i = 0$, since the other cases are treated similarly):

$$\frac{3v_{0jk} - 4v_{1jk} + v_{2jk}}{2\Delta x} = 0 \Longleftrightarrow 3v_{0jk} - 4v_{1jk} + v_{2jk} = 0.$$

If $(x_i, y_j, z_k) \in \Gamma$ the s-th equation of the linear system is obtained by discretizing the interface condition (36) on (x_i, y_j, z_k) with second order accuracy as follows (assume that $i = i^*$, since the other cases are treated similarly):

$$\frac{3v_{i^*,j,k} - 4v_{i^*+1,j,k} + v_{i^*+2,j,k}}{2\Delta x} - \frac{-3v_{i^*,j,k} + 4v_{i^*-1,j,k} - v_{i^*-2,j,k}}{2\Delta x} = 0.$$

$$\Longleftrightarrow 6v_{i^*,j,k} - 4v_{i^*+1,j,k} + v_{i^*+2,j,k} - 4v_{i^*-1,j,k} + v_{i^*-2,j,k} = 0.$$

For all the other grid points, namely (x_i, y_j, z_k) internal to Ω_i or Ω_e, the s-th equation of the linear system is obtained by discretizing (33) on (x_i, y_j, z_k) with central second order

accuracy as follows:

$$\left(2\varepsilon_{i,j,k}\left(\frac{1}{\Delta x^2}+\frac{1}{\Delta y^2}+\frac{1}{\Delta z^2}\right)+\alpha_{ijk}\right)v_{i,j,k}$$
$$-\frac{\varepsilon_{i-1/2,j,k}}{\Delta x^2}v_{i-1,j,k}-\frac{\varepsilon_{i+1/2,j,k}}{\Delta x^2}v_{i+1,j,k}-\frac{\varepsilon_{i,j-1/2,k}}{\Delta y^2}v_{i,j-1,k}$$
$$-\frac{\varepsilon_{i,j+1/2,k}}{\Delta y^2}v_{i,j+1,k}-\frac{\varepsilon_{i,j,k-1/2}}{\Delta z^2}v_{i,j,k-1}-\frac{\varepsilon_{i,j,k+1/2}}{\Delta z^2}v_{i,j,k+1}=f_{ijk},$$

where $\varepsilon_{ijk}=\varepsilon(x_i,y_j,z_k)$, $\varepsilon_{i+1/2,j,k}=\varepsilon(x_i+\Delta x/2,y_j,z_k)$, $\alpha_{ijk}=\alpha(x_i,y_j,z_k)$, $f_{ijk}=f(x_i,y_j,z_k)$.

References

Camiola, V. D., Mascali, G., and Romano, V. (2012). "Numerical simulation of a double-gate MOSFET with a subband model for semiconductors based on the maximum entropy principle". *Continuum Mechanics and Thermodynamics* **24**(4), 417–436. DOI: 10.1007/s00161-011-0217-6.

Camiola, V. D., Mascali, G., and Romano, V. (2013). "Simulation of a double-gate MOSFET by a non-parabolic energy-transport subband model for semiconductors based on the maximum entropy principle". *Mathematical and Computer Modelling* **58**(1), 321–343. DOI: 10.1016/j.mcm.2012.11.007.

Castiglione, T. and Muscato, O. (2017). "Non-parabolic band hydrodynamic model for silicon quantum wires". *Journal of Computational and Theoretical Transport* **46**(3), 186–201. DOI: 10.1080/23324309.2017.1318402.

Coco, A. and Russo, G. (2012). "Second order multigrid methods for elliptic problems with discontinuous coefficients on an arbitrary interface, I: one dimensional problems". *Numerical Mathematics: Theory, Methods and Applications* **5**(1), 19–42. DOI: 10.1017/S1004897900000209.

Coco, A. and Russo, G. (2013). "Finite-difference ghost-point multigrid methods on Cartesian grids for elliptic problems in arbitrary domains". *Journal of Computational Physics* **241**, 464–501. DOI: 10.1016/j.jcp.2012.11.047.

Coco, A. and Russo, G. (2018). "Second order finite-difference ghost-point multigrid methods for elliptic problems with discontinuous coefficients on an arbitrary interface". *Journal of Computational Physics* **361**, 299–330. DOI: 10.1016/j.jcp.2018.01.016.

Di Stefano, V. and Muscato, O. (2012). "Seebeck Effect in Silicon Semiconductors". *Acta Applicandae Mathematicae* **122**(1), 225–238. DOI: 10.1007/s10440-012-9739-6.

Ferry, D. K., Goodnick, S. M., and Bird, J. (2009). *Transport in nanostructures*. Cambridge University Press. DOI: 10.1017/CBO9780511626128.

Gnani, E., Reggiani, S., Gnudi, A., Parruccini, P., Colle, R., Rudan, M., and Baccarani, G. (2007). "Band-Structure Effects in Ultrascaled Silicon Nanowires". *IEEE Transactions on Electron Devices* **54**(9), 2243–2254. DOI: 10.1109/TED.2007.902901.

Guerfi, Y. and Larrieu, G. (2016). "Vertical Silicon Nanowire Field Effect Transistors with Nanoscale Gate-All-Around". *Nanoscale Research Letters* **11**, 210. DOI: 10.1186/s11671-016-1396-7.

Jin, S., Fischetti, M. V., and Tang, T.-W. (2007). "Modeling of electron mobility in gated silicon nanowires at room temperature: Surface roughness scattering, dielectric screening, and band nonparabolicity". *Journal of Applied Physics* **102**, 083715. DOI: 10.1063/1.2802586.

Lebon, G., Jou, D., and Casas-Vázquez, J. (2008). *Understanding Non-equilibrium Thermodynamics*. Springer-Verlag Berlin Heidelberg. DOI: 10.1007/978-3-540-74252-4.

Lenzi, M., Palestri, P., Gnani, E., Reggiani, S., Gnudi, A., Esseni, D., Selmi, L., and Baccarani, G. (2008). "Investigation of the Transport Properties of Silicon Nanowires Using Deterministic and

Monte Carlo Approaches to the Solution of the Boltzmann Transport Equation". *IEEE Transactions on Electron Devices* **55**(8), 2086–2096. DOI: 10.1109/TED.2008.926230.

Mascali, G. (2015). "A hydrodynamic model for silicon semiconductors including crystal heating". *European Journal of Applied Mathematics* **26**(4), 477–496. DOI: 10.1017/S0956792515000157.

Mascali, G. (2016). "A new formula for silicon thermal conductivity based on a hierarchy of hydrodynamical models". *Journal of Statistical Physics* **163**(5), 1268–1284. DOI: 10.1007/s10955-016-1509-9.

Mascali, G. (2017). "Thermal conductivity reduction by embedding nanoparticles". *Journal of Computational Electronics* **16**(1), 180–189. DOI: 10.1007/s10825-016-0934-y.

Mascali, G. and Romano, V. (2010). "Hydrodynamic subband model for semiconductors based on the maximum entropy principle". *Il Nuovo Cimento* **33C**(1), 155–163. DOI: 10.1393/ncc/i2010-10578-0.

Mascali, G. and Romano, V. (2012). "A non parabolic hydrodynamic subband model for semiconductors based on the maximum entropy principle". *Mathematical and Computer Modelling* **55**, 1003–1020. DOI: 10.1016/j.mcm.2011.09.026.

Muscato, O. and Castiglione, T. (2016). "Electron transport in silicon nanowires having different cross-sections". *Communications in Applied and Industrial Mathematics* **7**(2), 8–25. DOI: 10.1515/caim-2016-0003.

Muscato, O. and Castiglione, T. (2017). "A Hydrodynamic Model for Silicon Nanowires Based on the Maximum Entropy Principle". *Entropy* **18**, 368. DOI: 10.3390/e18100368.

Muscato, O. and Di Stefano, V. (2011a). "An Energy Transport Model describing heat generation and conduction in silicon semiconductors". *Journal of Statistical Physics* **144**, 171–197. DOI: 10.1007/s10955-011-0247-2.

Muscato, O. and Di Stefano, V. (2011b). "Heat generation and transport in nanoscale semiconductor devices via Monte Carlo and hydrodynamic simulations". *International Journal of Computations and Mathematics in Electrical* **30**(2), 519–537. DOI: 10.1108/03321641111101050.

Muscato, O. and Di Stefano, V. (2011c). "Hydrodynamic modeling of the electro-thermal transport in silicon semiconductors". *Journal of Physics A: Mathematical and Theoretical* **44**, 105501. DOI: 10.1088/1751-8113/44/10/105501.

Muscato, O. and Di Stefano, V. (2011d). "Local equilibrium and off-equilibrium thermoelectric effects in silicon semiconductors". *Journal of Applied Physics* **110**(9), 093706. DOI: 10.1063/1.3658016.

Muscato, O. and Di Stefano, V. (2012). "Hydrodynamic modeling of silicon quantum wires". *Journal of Computational Electronics* **11**(1), 45–55. DOI: 10.1007/s10825-012-0381-3.

Muscato, O. and Di Stefano, V. (2013). "Electro-thermal behaviour of a sub-micron silicon diode". *Semiconductor Science and Technology* **28**, 025021. DOI: 10.1088/0268-1242/28/2/025021.

Muscato, O. and Di Stefano, V. (2014). "Hydrodynamic simulation of a $n^+ - n - n^+$ silicon nanowire". *Continuum Mechanics and Thermodynamics* **26**, 197–205. DOI: 10.1007/s00161-013-0296-7.

Muscato, O. and Di Stefano, V. (2015). "Electrothermal transport in silicon carbide semiconductors via a hydrodynamic model". *SIAM Journal on Applied Mathematics* **75**(4), 1941–1964. DOI: 10.1137/140995623.

Muscato, O., Di Stefano, V., and Wagner, W. (2013). "A variance-reduced electrothermal Monte Carlo method for semiconductor device simulation". *Computers & Mathematics with Applications* **65**(3), 520–527. DOI: 10.1016/j.camwa.2012.03.100.

Muscato, O. and Wagner, W. (2016). "A class of stochastic algorithms for the Wigner equation". *SIAM Journal on Scientific Computing* **38**(3), A1483–A1507. DOI: 10.1137/16M105798X.

Muscato, O., Wagner, W., and Di Stefano, V. (2010). "Numerical study of the systematic error in Monte Carlo schemes for semiconductors". *ESAIM: Mathematical Modelling and Numerical Analysis* **44**(5), 1049–1068. DOI: 10.1051/m2an/2010051.

Muscato, O., Wagner, W., and Di Stefano, V. (2011). "Properties of the steady state distribution of electrons in semiconductors". *Kinetic & Related Models* **4**(3), 809–829. DOI: 10.3934/krm.2011.4.809.

Nehari, K., Cavassilas, N., Autran, J. L., Bescond, M., Munteanu, D., and Lannoo, M. (2006). "Influence of band structure on electron ballistic transport in silicon nanowire MOSFETs: An atomistic study". *Solid-State Electronics* **50**, 716–721. DOI: 10.1016/j.sse.2006.03.041.

Neophytou, N. and Kosina, H. (2011). "Atomistic simulations of low-field mobility in Si nanowires: Influence of confinement and orientation". *Physical Review B* **84**, 085313. DOI: 10.1103/PhysRevB.84.085313.

Neophytou, N., Paul, A., Lundstrom, M. S., and Klimeck, G. (2008). "Bandstructure Effects in Silicon Nanowire Electron Transport". *IEEE Transactions on Electron Devices* **55**(6), 1286–1297. DOI: 10.1109/TED.2008.920233.

Ossig, G. and Schürrer, F. (2008). "Simulation of non-equilibrium electron transport in silicon quantum wires". *Journal of Computational Electronics* **7**, 367–370. DOI: 10.1007/s10825-008-0238-y.

Ramayya, E. and Knezevic, I. (2010). "Self-consistent Poisson-Schrödinger-Monte Carlo solver: electron mobility in silicon nanowires". *Journal of Computational Electronics* **9**, 206–210. DOI: 10.1007/s10825-010-0341-8.

Ramayya, E., Vasileska, D., Goodnick, S., and Knezevic, I. (2008). "Electron transport in silicon nanowires: the role of acoustic phonon confinement and surface roughness scattering". *Journal of Applied Physics* **104**, 063711. DOI: 10.1063/1.2977758.

Singh, N., Agarwal, A., Bera, L. K., Liow, T. Y., Yang, R., Rustagi, S. C., Tung, C. H., Kumar, R., Lo, G. Q., Balasubramanian, N., and Kwong, D.-L. (2006). "High-performance fully depleted silicon nanowire (diameter $\leq$ 5 nm) gate-all-around CMOS devices". *IEEE Electron Device Letters* **27**(5), 383–386. DOI: 10.1109/LED.2006.873381.

Trellakis, A., Galik, T., Pacelli, A., and Ravaioli, U. (1997). "Iteration scheme for the solution of the two-dimensional Schrödinger-Poisson equations in quantum structures". *Journal of Applied Physics* **81**, 7880–7884. DOI: 10.1063/1.365396.

Wang, J. and Lundstrom, M. (2002). "Does source-to-drain tunneling limit the ultimate scaling of MOSFETs?" *International Electron Devices Meeting TECHNICAL DIGEST*, 707–710. DOI: 10.1109/IEDM.2002.1175936.

Zheng, Y., Rivas, C., Lake, R., Alam, K., Boykin, T. B., and Klimeck, G. (2005). "Electronic Properties of Silicon Nanowires". *IEEE Transactions on Electron Devices* **52**(6), 1097–1103. DOI: 10.1109/TED.2005.848077.

---

[a] Università degli Studi di Catania,
Dipartimento di Matematica e Informatica
Viale Andrea Doria 6 - 95125 Catania, Italy

[b] Oxford Brookes University,
Department of Mechanical Engineering and Mathematical Sciences
Wheatley campus, OX33 1HX Oxford GB

[*] To whom correspondence should be addressed | email: muscato@dmi.unict.it

Paper contributed to the conference entitled "Thermal theories of continua: survey and developments (Thermocon 2016)", which was held in Messina, Italy (19–22 April 2016) under the patronage of the *Accademia Peloritana dei Pericolanti*

Manuscript received 25 October 2017; published online 20 May 2019

© 2019 by the author(s); licensee *Accademia Peloritana dei Pericolanti* (Messina, Italy). This article is an open access article distributed under the terms and conditions of the Creative Commons Attribution 4.0 International License (https://creativecommons.org/licenses/by/4.0/).